Supporting Information

Functionalized Carbon Nanotube Mediated Transport in Membranes Containing Fixed-Site Carriers for Fast Pervaporation Desalination

Guang Yang,[†,‡] Zongli Xie,[,‡] Shixin Zhang,[‡,§] Huaili Zheng,[§] Kewei Cai,[‡] Marlene Cran,[†] Derrick Ng,[‡] Chunrui Wu[∥], Stephen Gray,[*,†]*

[†] *Institute for Sustainable Industries and Liveable Cities, Victoria University, PO Box 14428, Melbourne, Vic. 8001, Australia.*

[‡] *CSIRO Manufacturing, Private Bag 10, Clayton South, Vic. 3169, Australia.*

[§] *Key laboratory of the Three Gorges Reservoir Region's Eco-Environment, State Ministry of Education, Chongqing University, Chongqing 400045, P.R. China.*

[∥] *State Key Laboratory of Separation Membranes and Membrane Processes, Institute of Biological and Chemical Engineering, Tianjin Polytechnic University, Tianjin 300387, PR China*

Corresponding authors:

* *Email : stephen.gray@vu.edu.au;*

* *Email: zongli.xie@csiro.au;*

Supporting Note: XPS experimental details and curve-fit protocol

X-ray photoelectron spectroscopy (XPS) analysis was performed using an AXIS Nova spectrometer (Kratos Analytical Inc., Manchester, UK) with a monochromated Al Kα source at a power of 180 W (15 kV, 12 mA). The total pressure in the main vacuum chamber during analysis was typically between 10^{-9} and 10^{-8} mbar. Survey spectra were acquired at a pass energy of 160 eV and step size 0.5 eV. To obtain more detailed information about chemical structure, oxidation states etc., high resolution spectra were recorded from individual peaks at 40 eV pass energy and step size 0.1 eV, typically yielding a full width at half maximum (FWHM) of < 0.85 eV for the ester peak in PET during performance tests. The samples were drop-cast into shallow wells of a clean stainless steel sample holder and were analysed at a nominal photoelectron emission angle of 0º. Since the actual emission angle is ill-defined in the case of a rough surface topography (ranging from 0º to 90º) the sampling depth may range from 0 nm to approximate 10 nm.

Data processing was performed using CasaXPS processing software version 2.3.21 (Casa Software Ltd., Teignmouth, UK). All elements present were identified from survey spectra. The atomic concentrations of the detected elements were calculated using integral peak intensities and the sensitivity factors supplied by the manufacturer. Atomic concentrations of chemically different carbon species were determined by curve-fitting the C 1s peak. The experimentally obtained reference spectrum of pristine CNT was used as a fit component to represent graphitic species. In addition, four components (pseudo Voigt functions) were used to represent C-C and C-H species (C1 at approx. 285 eV), C-O based functional groups (C2; 286.5 eV), C=O and O-C-O based groups (C3; 288 eV), and O-C=O based functionalities (C4 at just above 289 eV). Binding energies were referenced to the C 1s peak at 284.5 eV graphitic carbon (CNTs).

The accuracy associated with quantitative XPS is ca. 10% - 15%. Precision (ie. reproducibility) depends on the signal/noise ratio but is usually much better than 5%. The latter is relevant when comparing similar samples.

Supporting Figures

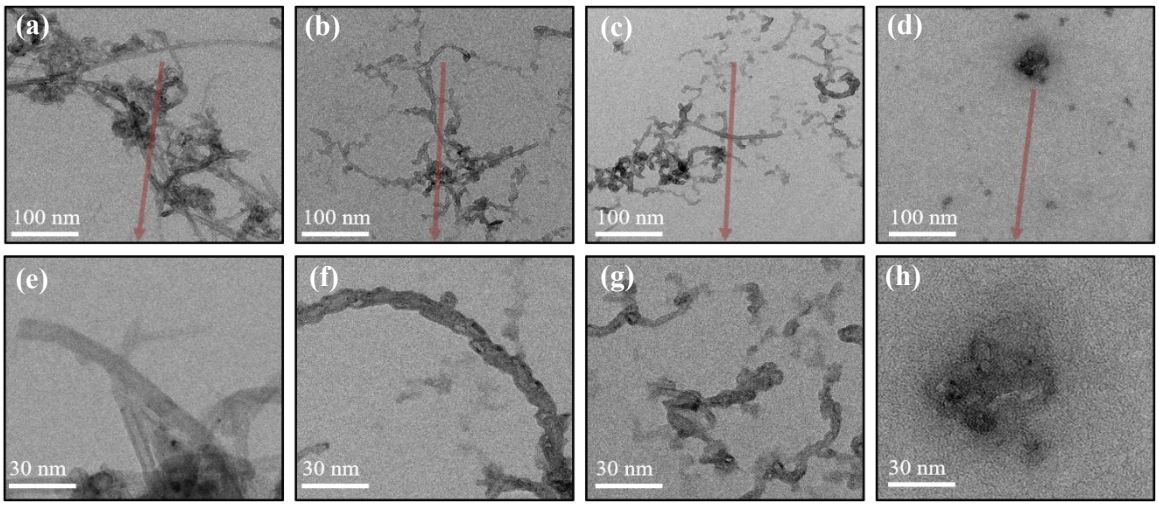

Figure S1. TEM images of the MWCNTs: (a) pristine MWCNTs, (b) ACNT2, (c) ACNT4 and (d) ACNT6. Images (e-h) correspond to (a-d), respectively.

In Figure S1, the morphology changes of the MWCNTs before and after chemical oxidation are presented using TEM. The pristine MWCNTs easily formed bundles or clumps (Figure S1a) because of their strong Van der Waals and π–π interactions.[1] For a single pristine MWCNT (Figure S1e), the TEM image revealed its multi-walled structure and smooth surface, in line with previous literature.[2] However, after the acid-treatment, the inclination to form entanglements was restrained by attaching oxygen-containing polar groups. As shown in Figure S1b and c, the ACNTs exhibited sinuous appearance as well as a better distribution state (less entangled) in the imaged section, showing promise for obtaining good dispersion in PVA. More specifically, the surface morphologies of ACNT2 (Figure S1f) and ACNT4 (Figure S1g) turned rougher than that of pristine MWCNTs. This could be regarded as evidence of the chemical modification by creating defects on the surface. The nanotube length was also found with relative reduction by extending the acid-treatment time. For the resulting MWCNTs in harsher condition (ACNT6), the average length of the tube was cut down

to less than 30 nm whereas masses of amorphous carbon materials possibly composed of oxidation debris could be seen. As such, the main tube structures of ACNTs were unexpectedly destroyed as a result of overreaction with acid mixtures.

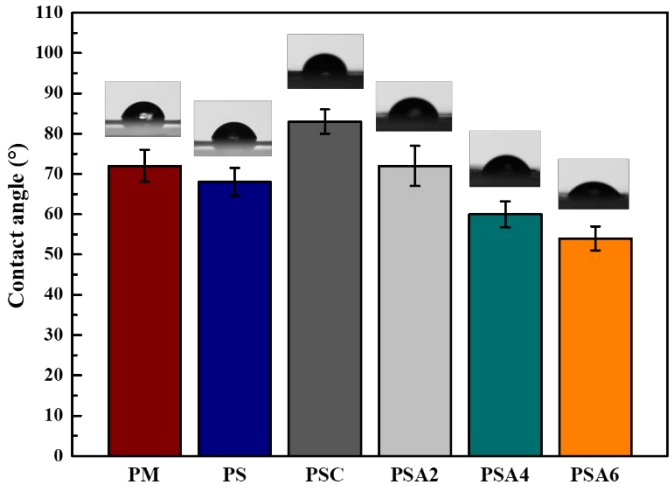

Figure S2. Water contact angles of the fabricated membranes.

Water contact angle tests were conducted to investigate the impacts of the pristine MWCNTs and acid-treated MWCNTs on the membrane surface hydrophilicity. As shown in Figure S2, PS had a slightly lower contact angle (68°) than PM (72°), which could be attributed to the sulfonic acid groups (from SSA) that were distributed on the membrane surface. After the incorporation of the pristine MWCNTs, the membrane surface exhibited reduced hydrophilicity with a contact angle of 83°. It is understandable that the hydrophobic nature of the pristine MWCNTs could enhance the hydrophobicity of the membrane. For the membranes with acid-treated MWCNTs, it can be seen that the membrane surfaces became more hydrophilic with the increased acid treatment time, i.e., 72° for PSA2, 60° for PSA4 and 54° for PSA6. As evidenced in the XPS results, the longer oxidation time rendered higher concentration of oxygen-containing groups on the MWCNTs. As a result, the water molecules were more likely to contact those hydrophilic groups that appeared on the membrane surface and thus exhibited lower contact angle values.

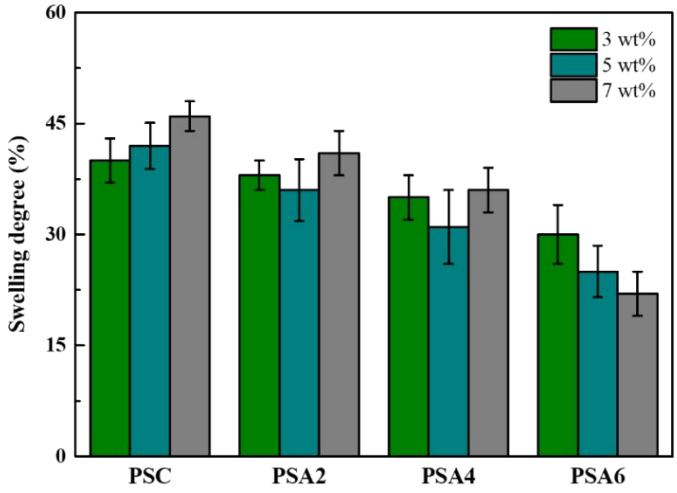

Figure S3. Swelling of membranes with different MWCNT or ACNT contents.

The swelling results are shown in Figure S3 where the swelling degrees of the PSC membranes increased with the pristine MWCNT content. This phenomenon could be attributed to the interfacial incompatibility and increased MWCNT agglomeration in the PVA matrix, creating more interfacial voids for accommodation of water molecules. For PSA2 and PSA4, with the MWCNT contents increasing, the swelling degrees first decreased to a minimum value at 5 wt% ACNT loading and then increased. The initial decrease is related with the interfacial interactions between ACNTs and PVA, restraining the mobility of PVA chains as evidenced in DSC and ATR-FTIR results. The increase in swelling at higher ACNT content of 7 wt% could be attributed to the potential agglomeration of ACNTs. For PSA6 membranes, the swelling degrees decreased continuously with the ACNT contents, indicating longer oxidation time rendered the ACNT6 with substantial oxygen-containing groups (evidenced in XPS results), leading to a good dispersion state even at high loading of 7 wt%. That resulted in increased interfacial interactions between ACNT6 and PVA that suppressed the mobility of PVA chains.

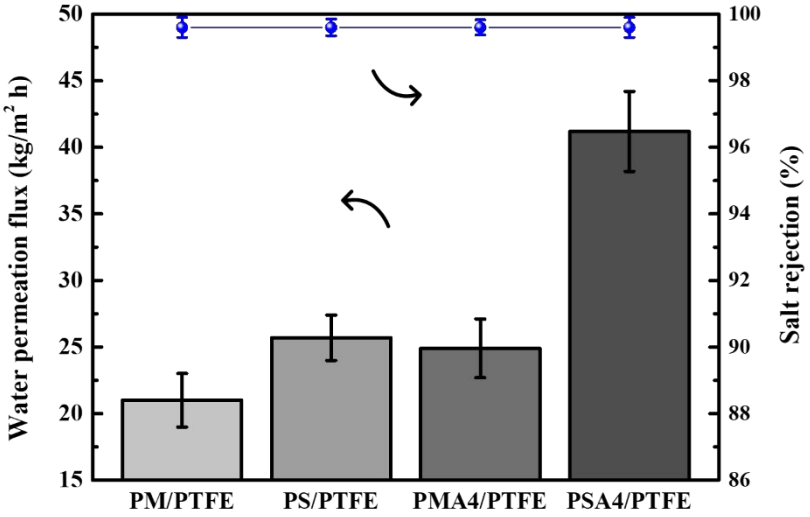

Figure S4. Separation performances of the membranes with or without ACNT4.

A PVA/MA/ACNT4 (5 wt% loading) film on PTFE substrate (referred to as PMA4/PTFE) was also fabricated through the same preparation process as PSA4 (except for using MA as the crosslinker) and subject to the PV desalination in the same conditions of 30 °C, 130 Pa and 35000 ppm NaCl as the feed. The separation performance of PMA4/PTFE was compared with those of PM/PTFE, PS/PTFE and PSA4/PTFE as shown in Figure S4. As can be seen, the incorporation of CNTs into the polymer matrix as occurred in PMA4 led to an increase of water permeation flux from 21.1 kg/m^2 h to 24.9 kg/m^2 h (18% flux increase) without decreasing the separation efficiency, which can be attributed to the specific transport property of CNTs and good interfacial compatibility with the polymer. The PS/PTFE membrane exhibited a 22% flux increase compared with PM/PTFE due to the facilitated transport agents. The PSA4/PTFE membrane showed 1.67 and 1.61 times of water fluxes compared with membranes containing either nanofillers or transport agents, i.e., PMA4/PTFE and PS/PTFE, respectively. In particular, the water flux of the PSA4/PTFE membrane was

1.97 times of that of PM/PTFE membrane (without transport agents and nanofillers). These results demonstrated that the combination of ACNTs and sulfonic acid groups in the polymer based membrane was more effective in flux enhancements than either component of ACNTs or sulfonic acid groups.

Table S1
Detailed information of the PV membranes and operating conditions.

Membrane	Thickness (μm)	Feed temp (°C)	Pressure (Pa)	NaCl (ppm)	Flux (kg/m^2 h)	Salt rejection (%)	Ref.
PVA/MA/silica	6	22	800	2000	6.93	99.5	3
S-PVA/PAN	0.8	30	100	35000	14.11	99.7	4
Polyetheramide	40	70	–	32000	0.56	99.99	5
Polyester	750	20	–	35000	7.1×10^{-3}	99.84	6
Carbon/silica	_	25	vacuum	35000	1.8	98	7
Cotton cellulose	30	40	20	40000	6.7	100	8
PVA/PSf	0.1	70	vacuum	30000	7.4	99.9	9
GOF-SSA	0.05	30	133	35000	22.2	99.9	10
GO/α-Al_2O_3	0.4	30	vacuum	35000	8.5	99.7	11
GO/PAN	0.03	30	100	35000	14.3	99.8	12
MXene/PAN	0.06	30	400	35000	48.2	99.5	13
PSA4/PTFE	0.7	30	130	35000	41.5	99.7	This work
PSA6/PTFE	0.7	30	130	35000	31.2	99.7	This work

Supporting References

(1) Perez, E. M.; Martin, N., π-π interactions in carbon nanostructures. *Chem. Soc. Rev.* **2015,** *44*, 6425-6433.

(2) Van Trinh, P.; Anh, N. N.; Tam, N. T.; Hong, N. T.; Hong, P. N.; Minh, P. N.; Thang, B. H., Influence of defects induced by chemical treatment on the electrical and thermal conductivity of nanofluids containing carboxyl-functionalized multi-walled carbon nanotubes. *RSC Adv.* **2017,** *7*, 49937-49946.

(3) Xie, Z.; Hoang, M.; Duong, T.; Ng, D.; Dao, B.; Gray, S., Sol–gel derived poly(vinyl alcohol)/maleic acid/silica hybrid membrane for desalination by pervaporation. *J. Membr. Sci.* **2011,** *383*, 96-103.

(4) Liang, B.; Li, Q.; Cao, B.; Li, P., Water permeance, permeability and desalination properties of the sulfonic acid functionalized composite pervaporation membranes. *Desalination* **2018,** *433*, 132-140.

(5) Zwijnenberg, H.; Koops, G.; Wessling, M., Solar driven membrane pervaporation for desalination processes. *J. Membr. Sci.* **2005,** *250*, 235-246.

(6) Sule, M.; Jiang, J.; Templeton, M.; Huth, E.; Brant, J.; Bond, T., Salt rejection and water flux through a tubular pervaporative polymer membrane designed for irrigation applications. *Environ. Technol.* **2013,** *34*, 1329-39.

(7) Duke, M. C.; Mee, S.; da Costa, J. C., Performance of porous inorganic membranes in non-osmotic desalination. *Water Res.* **2007,** *41*, 3998-4004.

(8) Kuznetsov, Y. P.; Kruchinina, E. V.; Baklagina, Y. G.; Khripunov, A. K.; Tulupova, O. A., Deep desalination of water by evaporation through polymeric membranes. *Russ. J. Appl. Chem.* **2007,** *80*, 790-798.

(9) Chaudhri, S. G.; Rajai, B. H.; Singh, P. S., Preparation of ultra-thin poly(vinyl alcohol) membranes supported on polysulfone hollow fiber and their application for production of pure water from seawater. *Desalination* **2015,** *367*, 272-284.

(10) Yang, G.; Xie, Z.; Cran, M.; Ng, D.; Easton, C. D.; Ding, M.; Xu, H.; Gray, S., Functionalizing graphene oxide framework membranes with sulfonic acid groups for superior aqueous mixture separation. *J. Mater. Chem. A* **2019,** *7*, 19682-19690.

(11) Xu, K.; Feng, B.; Zhou, C.; Huang, A., Synthesis of highly stable graphene oxide membranes on polydopamine functionalized supports for seawater desalination. *Chem. Eng. Sci.* **2016,** *146*, 159-165.

(12) Liang, B.; Zhan, W.; Qi, G.; Lin, S.; Nan, Q.; Liu, Y.; Cao, B.; Pan, K., High performance graphene oxide/polyacrylonitrile composite pervaporation membranes for desalination applications. *J. Mater. Chem. A* **2015,** *3*, 5140-5147.

(13) Liu, G.; Shen, J.; Liu, Q.; Liu, G.; Xiong, J.; Yang, J.; Jin, W., Ultrathin two-dimensional MXene membrane for pervaporation desalination. *J. Membr. Sci.* **2018,** *548*, 548-558.